Segregations and desorptions of Ge atoms in nanocomposite $Si_{1-x}Ge_x$ films during high-temperature annealing

Yu Wang(汪煜)[1], Meng Yang(杨濛)[1], Gang Wang(王刚)[1], Xiao-Xu Wei(魏晓旭)[1], Jun-Zhuan Wang(王军转)[1], Yun Li(李昀)[1], Ze-Wen Zou(左则文)[2], You-Dou Zheng(郑有炓)[1], and Yi Shi(施毅)[1,†]

[1] *Key Laboratory of Advanced Photonic and Electronic Materials and School of Electronic Science and Engineering, Nanjing University, Nanjing* 210093, *China*

[2] *College of Physics and Electronics Information, Anhui Normal University, Wuhu* 241000, *China*

(Received 18 August 2017; revised manuscript received 31 August 2017; published online 20 October 2017)

Nanocomposite $Si_{1-x}Ge_x$ films are deposited by dual-source jet-type inductively coupled plasma chemical vapor deposition (jet-ICPCVD). The segregations and desorptions of Ge atoms, which dominate the structural evolutions of the films during high-temperature annealing, are investigated. When the annealing temperature (T_a) is 900 °C, the nanocomposite $Si_{1-x}Ge_x$ films are well crystallized, and nanocrystals (NCs) with the core-shell structure form in the films. After being annealed at 1000 °C (above the melting point of bulk Ge), Ge atoms accumulate on the surfaces of Ge-rich films, whereas pits appear on films with lower Ge content, resulting from desorption. Meanwhile, voids are observed in the films. A cone-like structure involving the percolation of the homogeneous clusters and the crystallization of NCs enhances Ge segregation.

Keywords: $Si_{1-x}Ge_x$, annealing, segregation, desorption

PACS: 68.55.–a, 68.55.A– **DOI:** 10.1088/1674-1056/26/12/126801

1. Introduction

SiGe nanostructured materials have been extensively studied for more than two decades. Thus far, SiGe has been used in the fields of microelectronics and optoelectronics as heterojunction bipolar transistors,[1–3] infrared detectors[4,5] and thin-film solar cells.[6–8] Moreover, nanostructured SiGe shows a considerable prospect of using it as thermoelectric material.[9,10] Recently, enhancements in thermoelectric figure-of-merit were reported in the nanocomposite SiGe alloys.[11,12] The thermal conductivity is reduced due to the boundary phonon-scattering at the increased interface of the nanocomposite sample. However, the electrical conductivity drops and degrades the thermoelectric figure-of-merit. To improve the electrical conductivity, high-temperature treatments, such as spark-plasma sintering[13] and hot-pressing,[14] are conducted. With thermal treatment, the density and crystalline fraction of nanocomposite grains increase. Consequently the electrical conductivity is enhanced. With ambient temperature rising, the ability of an atom to migrate in the nanocomposite SiGe alloy is greatly enhanced due to the effects of the interface, strain and element aggregation, and results in the segregation and desorption of Ge atoms. Consequently, the structural and morphological transformation present the migrations of atoms, which affects the performance of nanocomposite SiGe alloy serving as a thermoelectric material.

Many efforts have been made to fabricate nanocomposite SiGe materials. Gresback *et al.*,[15] Pi and Kortshagen[16] have synthesized freestanding SiGe alloy nanocrystals (NCs) by the plasma method. Yang *et al.* adjusted the proportion of Ge and Si sources in magnetron sputtering and obtained complex films containing various crystalline structures, namely, Ge nanocrystals, Ge-SiGe core-shell, and nc-$Si_{1-x}Ge_x$ alloy.[17] In our previous work, a deposition technique that combined very high-frequency inductively coupled plasma with gas-jet (jet-ICPCVD) has been developed for high-rate depositions of Si and Ge films.[18] With further improvement, a dual-source structure was added to the system for depositing the nanocomposite SiGe films.[19] This structure provides different residence times for SiH_4 and GeH_4. To be specific, GeH_4 has a longer residence time, and is more likely to dissociate.[20] Meanwhile, the longer residence time also provides greater probability for Ge precursors to nucleate,[21] and contributes to the formation of localized micro-clusters in the film. In the present work, nanocomposite SiGe films are deposited by dual-source jet-ICPCVD. Furthermore, the internal structures and surface morphologies of $Si_{1-x}Ge_x$ films are investigated to understand the influence of atomic migrations during high-temperature annealing (up to 1000 °C).

2. Experimental details

Nanocomposite $Si_{1-x}Ge_x$ films were deposited on silicon dioxide and quartz substrates by dual-source jet-ICPCVD

†Corresponding author. E-mail: yshi@nju.edu.cn

© 2017 Chinese Physical Society and IOP Publishing Ltd

(Fig. 1). The gas H_2 served as a source of plasma, and the H_2 flow rate was controlled in a range from 40 sccm to 150 sccm. The flow rates of SiH_4 (20% diluted in H_2) and GeH_4 (20% diluted in H_2) were adjusted from 0 sccm to 6 sccm and 0 sccm to 8 sccm, respectively. The chamber pressure was regulated from 40 Pa to 130 Pa, and the radio-frequency (RF) power was controlled from 50 W to 150 W.

The $Si_{1-x}Ge_x$ films were annealed in an ambient vacuum after being deposited. The annealing temperature (T_a) was in the range from 300 °C to 1000 °C, and the annealing times (t_a) were 60 s, 120 s, and 300 s. Characterizations of the microstructures were conducted by Raman spectroscopy (Horiba HR800), x-ray photoelectron spectroscopy (XPS, PHI 5000 Versa Probe), energy dispersive spectroscopy (EDS, Horiba EX-250), scanning electron microscopy (SEM, Joel 7000F), and transmission electron microscopy (TEM, TECNAI G2 20).

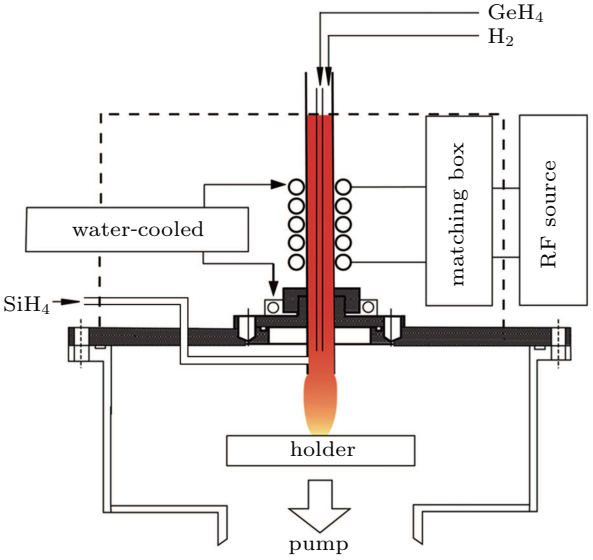


Fig. 1. (color online) Schematic diagram of the dual-source jet-ICPCVD system.

3. Results and discussion

Figure 2 shows the Raman spectra of the Ge-rich $Si_{0.3}Ge_{0.7}$ films after being annealed at 300 °C–900 °C for 300 s. When $T_a = 500$ °C, peaks appear at 285, 396.5, and 465 cm^{-1}, corresponding to the optical phonon modes of Ge–Ge, Ge–Si and Si–Si in the $Si_{1-x}Ge_x$ alloy, which implies the formation of NCs. As the T_a was raised to 800 °C, the intensities of these peaks are enhanced, and slight blue-shifts occur in all phonon modes, indicating that the density and size of NCs increase. Meanwhile, a weak peak at 440 cm^{-1} emerges. According to the work by Alonso and Winer[22] and Liu *et al.*,[23] this peak is ascribed to the localized vibration of the Si–Si bond surrounded by Ge atoms. The frequency of the Si–Si bond vibration is red-shifted when most of the neighboring Si atoms are replaced by heavier Ge atoms. When T_a is increased from 800 °C to 900 °C, both the intensities and frequencies of the phonon peaks obviously change. Figure 3 shows the TEM image of the Ge-rich sample after being annealed at 900 °C for 300 s. A large number of NCs with sizes of tens of nanometers can be observed, indicating that the film is well crystallized. The detailed analysis shows the structural evolutions of the Ge-rich $Si_{1-x}Ge_x$ films during thermal annealing below 900 °C.[19] Many Ge-rich regions exist in the as-deposited films, and in the initial stage of crystallization at $t_a = 500$ °C, these regions act as crystallization centers to form Ge NCs. As T_a is continually increased, due to the segregation of Ge and relaxation of strain, a transformation occurs from micro-clusters to composite NCs with Ge cores and SiGe shells. By Monte Carlo simulations, Tzoumanekas and Kelires suggested that homogeneous atoms in an amorphous SiGe alloy tend to cluster in the annealing process, resulting in a similar structure.[24,25]

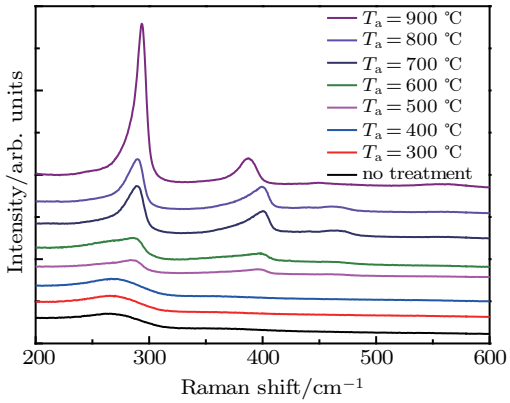


Fig. 2. (color online) Raman spectra of the $Si_{0.3}Ge_{0.7}$ films annealed at different values of T_a.

According to the phase diagram, the melting point of the $Si_{1-x}Ge_x$ alloy is between those of Si and Ge and varies with the composition of $Si_{1-x}Ge_x$. A large co-existence zone exists between solid and liquid phases, which indicates that the SiGe NCs is a mixture of liquid and solid when T_a exceeds the melting point of bulk Ge (938 °C). To investigate the atomic migration behavior and its influence on the $Si_{1-x}Ge_x$ films at high temperatures, we raise T_a to 1000 °C. Figure 4(a) shows the Raman spectrum of the $Si_{0.3}Ge_{0.7}$ film annealed at 1000 °C for 300 s. The Ge–Ge mode peak located at 299.5 cm^{-1} is sharp and highly symmetrical, implying that Ge is well crystallized. The Si–Si mode is extremely weak relative to the Ge–Ge mode and remains localized as shown in the inset of Fig. 4(a). The Ge–Si mode is much more complicated and can be fitted to four sub-peaks located at 379, 394, 393, and 400 cm^{-1}, respectively (Fig. 4(b)). We assume that the sub-peaks below 400 cm^{-1} are related to localized Si-Ge bonds surrounded by different numbers (1, 2 or 3) of Ge atoms, which is similar to the scenario of localized Si–Si bonds. For the further analy-

sis of the surface morphology, an SEM measurement is conducted on the annealed $Si_{0.3}Ge_{0.7}$ film. Figure 5(a) shows the SEM image of the surface, which clearly displays a layer of melted matter with an underlying porous structure. By EDS mapping (Fig. 5(b)), the melted layer is confirmed to be Ge. Hence, based on the experimental results, a portion of the Ge atoms transfer to the film surface and accumulate in the annealing process. When T_a increases to above the melting point of Ge, the accumulated Ge atoms are molten and lay over the film surface.

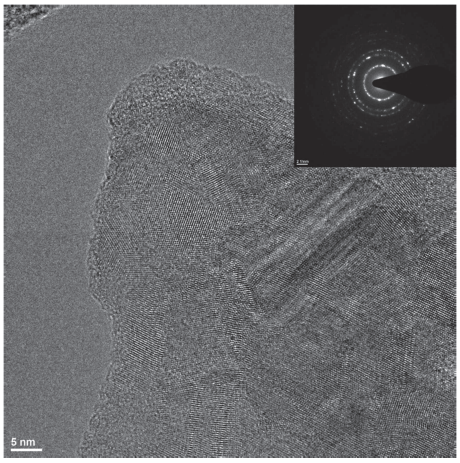


Fig. 3. TEM image and the diffraction pattern (inset) of Ge-rich SiGe film after thermal annealing at 900 °C for 300 s.

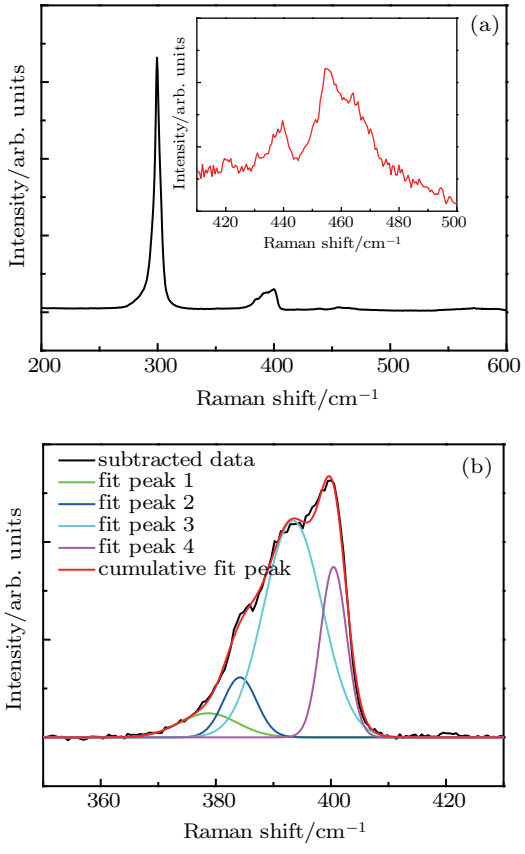


Fig. 4. (color online) (a) Raman spectrum of the $Si_{0.3}Ge_{0.7}$ film annealed at 1000 °C. The inset shows the zoomed spectrum of the Si–Si mode. (b) Multiple peak fitting of the Ge–Si mode.

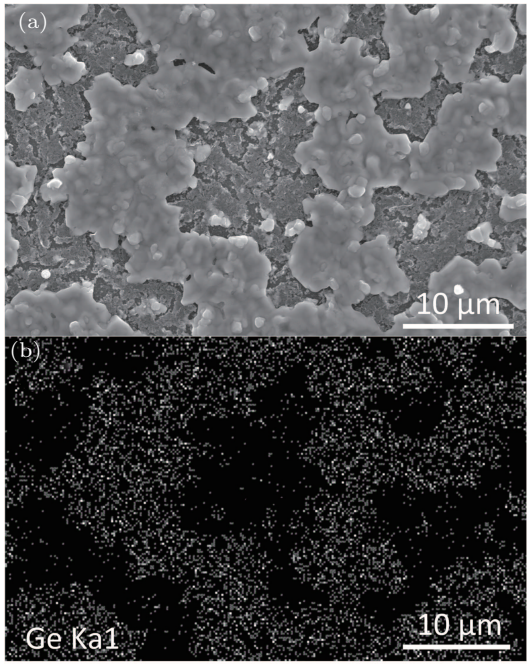


Fig. 5. (a) SEM image and (b) EDS mapping of the $Si_{0.3}Ge_{0.7}$ film annealed at 1000 °C.

To investigate the influence of the atomic composition, another set of $Si_{1-x}Ge_x$ films with lower Ge content ($x = 0.4$) is deposited and then annealed at 1000 °C for 60, 120, and 300 s. In the Raman spectra shown in Fig. 6, peaks at 286, 404, and 490 cm^{-1} indicate that the film is well crystallized after being annealed at 1000 °C for 60 s. As t_a is prolonged to 300 s, the intensities of the Ge–Ge and Ge–Si modes obviously increase, and the frequency of the Ge–Ge mode is slightly blue-shifted to 287 cm^{-1}, revealing that both the density and the size of the NCs in the film increase with t_a increasing. The intensity of the Si–Si mode shows no obvious change, whereas the frequency of the Si–Si mode is red-shifted to 482.5 cm^{-1}, and a new localized Si–Si mode emerges at 446 cm^{-1}. These results indicate that the Si atoms prefer to disperse into the film rather than form Si-rich NCs. SEM measurements are used to investigate the morphologies and structures of the $Si_{1-x}Ge_x$ films. In Fig. 7, pits with diameters of 1 μ–2 μm are observed on the surface of the $Si_{0.6}Ge_{0.4}$ film annealed at 1000 °C for 300 s (Figs. 7(a) and 7(b)], which is different from that observed on the Ge-rich films as shown in Fig. 5(a). Meanwhile, many voids with sizes of tens of nanometers are embedded in the annealed film. To analyze the variation of the atomic composition on the film surfaces, the Ge concentration as a function of annealing time t_a is determined by EDS and XPS as plotted in Fig. 8. The XPS data indicate that the Ge concentration evidently decreases as t_a increases after annealing the film at 1000 °C. In general, the area that can be probed by XPS is confined to a layer with a certain thickness (approximately 2 μm–5 nm) on the top of the film surface. According to the XPS results, we infer that Ge desorption occurs in the film surface region during being annealed at 1000 °C, which is

attributed to evaporation in previous reports.[26] However, the EDS data show a different trend with respect to the Ge concentration, indicating a slight Ge enrichment when t_a is 60 s. Since the probing depth of EDS probes is much deeper than that of XPS, we can assume that a portion of the Ge atoms segregate from the bulk to the surface of the film. Upon increasing t_a, the Ge concentration drops to the original value before annealing. These results clearly indicate that an equilibrium is present between Ge segregation and desorption.

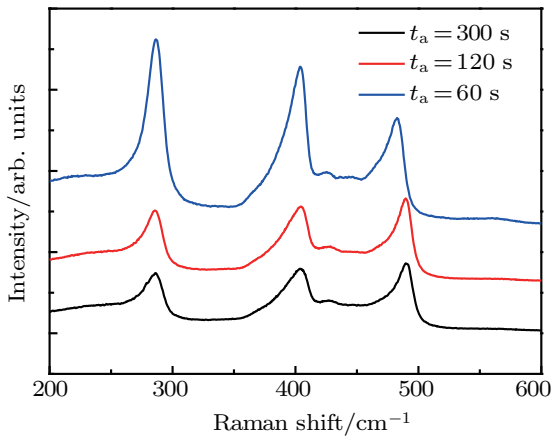


Fig. 6. (color online) Raman spectra of the $Si_{0.6}Ge_{0.4}$ films annealed at 1000 °C for different values of t_a.

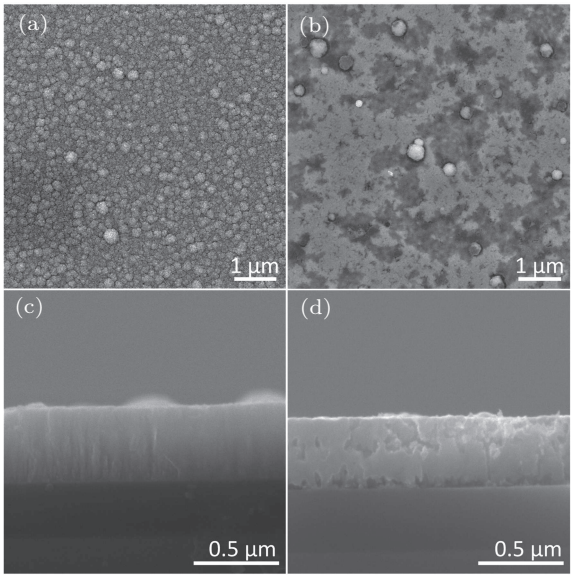


Fig. 7. ((a) and (b)) SEM images of the surface of the $Si_{0.6}Ge_{0.4}$ film before and after being annealed. ((c) and (d)) Cross-sectional SEM images before and after annealing the $Si_{0.6}Ge_{0.4}$ film.

The Ge atom segregation phenomenon on the $Si_{1-x}Ge_x$ nanocomposite surface is driven by the different covalent radii and surface energies of Ge and Si.[27–29] From the cross-sectional SEM image of the crystallized $Si_{1-x}Ge_x$ film shown in Fig. 9, cone-like crystalline grains are observed. In general, NCs grow via nucleation on a seed in the amorphous phase.[30] For the $Si_{1-x}Ge_x$ films discussed in this work, the Ge-rich regions act as nucleation seeds during crystallization. As the annealing process proceeds, increasingly more NCs are absorbed to form cone-like grains, which provides sufficient vertical interfaces as intermediate paths for segregation. First, Ge atoms transfer to the grain boundary and then travel toward the film surface along the boundary. Therefore, the Ge atom migration is enhanced due to the much faster surface diffusion than bulk diffusion.[31]

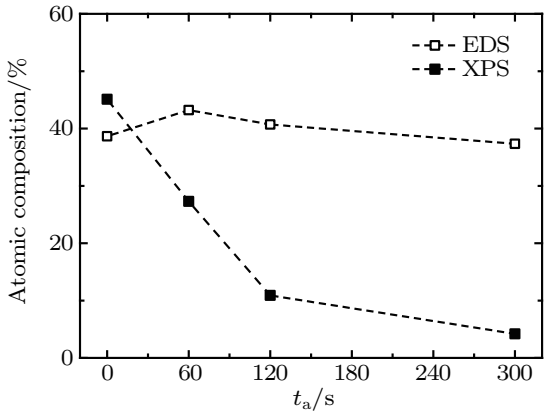


Fig. 8. EDS and XPS measured Ge atomic compositions as a function of t_a.

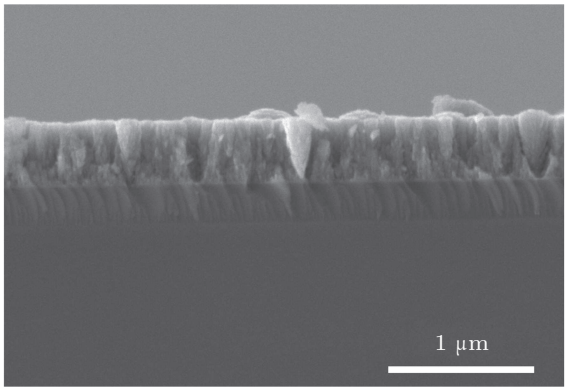


Fig. 9. Cross-sectional SEM image of the $Si_{1-x}Ge_x$ film annealed at 900 °C.

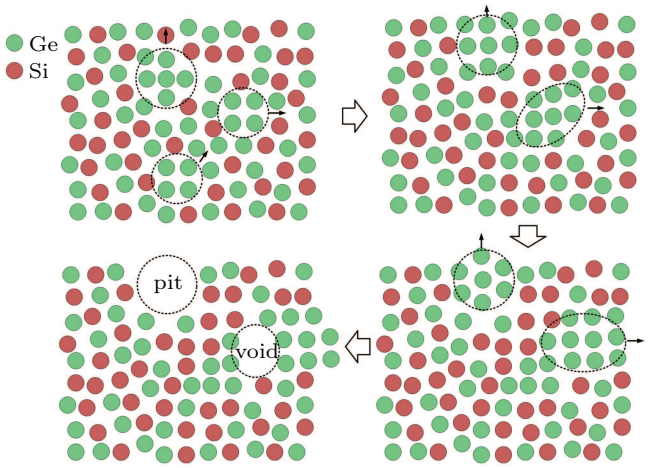


Fig. 10. (color online) Schematic diagrams of the formation of pits and voids in the SiGe film.

A mechanism involving the structural and morphological evolutions is proposed. As depicted in Fig. 10, Ge atoms segregate from the bulk to the surface, and simultaneously, Ge desorption to the vapor phase occurs on the surface during

high-temperature annealing. In the Ge-rich film, the segregation rate is higher than the desorption rate, and therefore, Ge atoms accumulate and are melted at 1000 °C. In the film with lower Ge content, the segregation rate is lower because the density of Ge–Si bonds increases, and the Ge–Si bonds are stronger than the Ge–Ge bonds. Accordingly, a net loss of Ge atoms occurs, and pits form on the surface. Since Ge atoms continuously transfer to the surface, voids form in all the films due to Ge atom migration.

4. Conclusions

The $Si_{1-x}Ge_x$ films are deposited by dual-source jet-ICPCVD to investigate the behaviors of nanostructured $Si_{1-x}Ge_x$ films during high-temperature annealing. When $T_a \leq 900$ °C, the $Si_{1-x}Ge_x$ films are well crystallized, and core-shell structures form as the effects of segregation and strain relaxation. As T_a increases to 1000 °C, a mechanism involving Ge segregation from the bulk to the surface and desorption from the surface is proposed to explain the structural and surface morphological evolutions. In the Ge-rich film, Ge atoms accumulate and are melted on the surface. In the film with a lower Ge content, pits form on the surface because Ge desorption is faster than segregation. Voids appear in films due to the loss of Ge atoms. The cone-like crystalline grains formed upon annealing enhance the Ge atom migration. The present work is helpful in understanding the thermal stabilities of nanostructured SiGe materials and guide us in further exploring their applications.

References

[1] Fu Q, Zhang W R, Jin D Y, Ding C B, Zhao Y X and Lu D 2014 *Chin. Phys. B* **23** 114402

[2] Schmidt J, Korn J, Fischer G G and Sorge R 2017 *IEEE Trans. Nucl. Sci.* **64** 1037

[3] Dwivedi A D D, Chakravorty A, D'esposito R, Sahoo A K, Fregonese S and Zimmer T 2016 *Solid-State Electronics* **115** 1

[4] Durmaz H, Sookchoo P, Cui X, Jacobson R B, Savage D E, Lagally M G and Paiella, R 2016 *ACS Photonics* **3** 1978

[5] Ali D and Richardson C J 2014 *Appl. Phys. Lett.* **105** 031116

[6] Li T T, Yang T, Fang J, Zhang D K, Sun J, Wei C C, Xu S Z, Wang G C, Liu C C, Zhao Y and Zhang X D 2016 *Chin. Phys. B* **25** 046101

[7] Ganguly G, Ikeda T, Nishimiya T, Saitoh K, Kondo M and Matsuda A 1996 *Appl. Phys. Lett.* **69** 4224

[8] Yan B, Zhao L, Chen J, Wang G, Diao H, Mao Y and Wang W 2013 *Vacuum* **89** 43

[9] Vining C B, Laskow W, Hanson J O, Van der Beck R R and Gorsuch P D 1991 *J. Appl. Phys.* **69** 4333

[10] Rowe D M, Shukla V S and Savvides N 1981 *Nature* **290** 765

[11] Joshi G, Lee H, Lan Y C, Wang X W, Zhu G H, Wang D Z, Gould R W, Cuff D C, Tang M Y, Dresselhaus M S, Chen G and Ren Z F 2008 *Nano Lett.* **8** 4670

[12] Wang X W, Lee H, Lan Y C, Zhu G H, Joshi G, Wang D Z, Yang J, Muto A J, Tang M Y, Klatsky J, Song S, Dresselhaus M S, Chen G and Ren Z F 2008 *Appl. Phys. Lett.* **93** 193121

[13] Xie W, Wang S, Zhu S, He J, Tang X, Zhang Q and Tritt T M 2013 *J. Mater. Sci.* **48** 2745

[14] Poudel B, Hao Q, Ma Y, Lan Y C, Minnich A, Yu B, Yan X, Wang D Z, Muto A, Vashaee D, Chen X Y, Liu J M, Dresselhaus M S, Chen G and Ren Z F 2008 *Science* **320** 634

[15] Gresback R, Holman Z and Kortshagen U 2007 *Appl. Phys. Lett.* **91** 093119

[16] Pi X D and Kortshagen U 2009 *Nanotechnology* **20** 295602

[17] Yang Y M, Wu X L, Siu G G, Huang G S, Shen J C and Hu D S 2004 *J. Appl. Phys.* **96** 5239

[18] Zuo Z W, Wang Y, Lu J, Wang J J, Pu L, Shi Y and Zheng Y D 2012 *Vacuum* **86** 924

[19] Wang Y, Yang M, Wang G, Wei X X, Wang J Z, Li Y, Zuo Z W, Zheng Y D and Shi Y 2015 *AIP Advances* **5** 117127

[20] Murley D T, Gibson R A G, Dunnett B, Goodyear A and French I D 1995 *J. Non-Cryst. Solids* **187** 324

[21] Ifuku T, Otobe M, Itoh A and Oda S 1997 *Jpn. J. Appl. Phys.* **36** 4031

[22] Alonso M I and Winer K 1989 *Phys. Rev. B* **39** 10056

[23] Liu L Z, Wu X L, Shen J C, Li T H, Gao F and Chu P K 2010 *Chem. Commun.* **46** 5539

[24] Tzoumanekas C and Kelires P C 2000 *J. Non-Cryst. Solids* **266** 670

[25] Tzoumanekas C and Kelires P C 2003 *Appl. Phys. Lett.* **82** 4681

[26] Zhang Z, Pan J S, Zhang J and Tok E S 2010 *PCCP* **12** 7171

[27] Walther T, Humphreys C J and Cullis A G 1997 *Appl. Phys. Lett.* **71** 809

[28] Fukatsu S, Fujita K, Yaguchi H, Shiraki Y and Ito R 1991 *Appl. Phys. Lett.* **59** 2103

[29] Tok E S, Woods N J and Zhang J 2000 *J. Cryst. Growth* **209** 321

[30] Vallat-Sauvain E, Kroll U, Meier J, Shah A and Pohl J 2000 *J. Appl. Phys.* **87** 3137

[31] Heitjans P and Kärger J (eds) 2006 *Diffusion in condensed matter: methods, materials, models* (Berlin: Springer Science & Business Media) p. 331